Semiclassical treatment of quantum propagation with nonlinear classical dynamics: A third-order thawed Gaussian approximation

Lucas Kocia*
Department of Chemistry and Chemical Biology, Harvard University, Cambridge, Massachusetts 02138, USA

Anna Klales
Department of Physics, Harvard University, Cambridge, Massachusetts 02138, USA

(Received 3 February 2016; revised manuscript received 24 May 2016; published 14 September 2016)

The time-dependent WKB approximation for a coherent state is expanded to third order around a guiding real trajectory, allowing for the novel treatment of nonlinearity in its semiclassical dynamics, which is generally present in all physical systems far from the classical regime. The result is a closed-form solution consisting of a linear combination of Airy functions and their derivatives multiplied by an exponential. The expression's ability to capture nonlinearity is demonstrated by examining the autocorrelation of initial coherent states in anharmonic systems with few to many contributing periodic orbits. Its accuracy is compared to the quadratic expansion and found to be superior in regimes of $\hbar$ where the curvature begins to be significant, as expected. Moreover, the expression is shown to be a real-trajectory uniformization over two coalescing saddle points that are emblematic of significant curvature. This extends real-trajectory time-dependent wave-packet semiclassical methods to highly anharmonic systems for the first time and establishes their regime of validity.

DOI: 10.1103/PhysRevE.94.032211

I. INTRODUCTION

The Feynman path integral provides a clear prescription for finding the quantum dynamics of states [1,2]. Unfortunately, it is exactly solvable in only a few simple cases, and so its semiclassical treatment is often considered instead. There has been much recent work on this topic, ranging from so-called "initial-value" representations [3–6], coupled multiconfigurational Gaussian methods [7,8], Bohmian mechanics [9], frozen Gaussian dynamics [10], Wigner formulations [11], and thawed Gaussian dynamics [12,13]. The direction considered here is most closely related to the last topic.

A variational expansion of the Feynman path integral up to second order in $\hbar$ produces the time-dependent Wentzel-Kramers-Brillouin (WKB)—the van Vleck–Morette–Gutzwiller (vVMG) propagator [14–16]—which reduces the number of trajectories that are considered to the set of only the (real or complex) classical trajectories between two manifolds, along with their action S and stability $\partial^2 S/\partial q' \partial q$. The position state representation of vVMG is

$$G^{\mathrm{vVMG}}(q,q',t) = \frac{1}{\sqrt{2\pi i\hbar}} \sum_{\mathrm{paths}} \left(\frac{\partial^2 S(q,q',t)}{\partial q \partial q'} \right)^{1/2} \times \exp\left[\frac{i}{\hbar} S(q,q',t) \right], \quad (1)$$

where q' and q are the initial and final positions, respectively, for time t.

When considering the propagation of states in time, it is necessary to expand their semiclassical propagator around guiding time-dependent trajectories [17,18] that approximate the local parts of the state that are of interest. Formally, these guiding trajectories should correspond to saddle points obtained by evaluating the integral between the vVMG propagator and a particular state by the method of steepest descents. When this expansion is done to quadratic order, the dynamics near guiding trajectories are linearized and the neighboring part of the state remains well approximated for any time with sufficiently small $\hbar$, or equivalently, for any $\hbar$ for a sufficiently short time. Even when the dynamics of the classical density are globally highly nonlinear in phase space, local pieces on the order of $\hbar$ can often still be linear and well captured, as has been shown for the Coulombic potential [19] and the stadium billiard [20]. This corresponds to the regime when the saddle points are sufficiently well separated from each other with respect to $\hbar$.

However, for larger $\hbar$, nonlinearities become important even at the local scale, and an expansion to higher than second order around the guiding trajectories becomes necessary. Such curvature is evidenced by two (or more) saddle points coming close enough together so that the area they encompass is on the order of $\hbar$. This causes the integration by the method of steepest descents to fail. In both prior studies, hairpins in phase space—highly curved manifolds—had to be avoided for this reason [19,20]. Such curvature is a general feature of almost any physically relevant system away from the classical regime. Therefore, there is a great need for a treatment that handles pervasive nonlinearity in phase space and coalescing saddle points uniformly; this is called a "uniformization." Related efforts have relied on many-trajectory uniformization [21] to address this issue.

In this paper, we will introduce a real-trajectory uniformization of the semiclassical dynamics of coherent states. This is the next order cubic treatment of the "off-centered thawed Gaussian approximation" [22]. It can also be described as a uniformization over real trajectories that approximates the time-dependent WKB treatment of Gaussians known as generalized Gaussian wave packet dynamics (GGWPD) [23,24]. As we will explain, the real trajectories can be viewed as an approximation to the generally complex trajectories

*To whom correspondence should be addressed: lkocia@fas.harvard.edu

 ©2016 American Physical Society

necessary in GGWPD. However, since they are real, they are far easier to find and use.

Unfortunately, many cubic expansions of this nature behave badly when taken to higher than second order, and fewer still have closed-form simple solutions. Will including the dynamics up to third order be a nonasymptotic expansion and therefore actually produce less accurate results? Is it still possible, as in earlier work, to calculate correlations of wave packets by summing orbit contributions based on their phase-space intersections?

II. DERIVATION OF THE CUBIC APPROXIMATION

As mentioned in the Introduction, in this paper we will consider coherent states—Gaussian wave packets in position and momentum space—whose representative classical densities are localized in phase space. To examine our higher-order expansion around guiding trajectories, we will work in one dimension and determine the time propagation of the initial Gaussian wave packet:

$$\Psi_\beta(q,0) = \sqrt[4]{\frac{1}{\pi\sigma^2}} \exp\left\{\frac{i}{\hbar}\left[\xi(q-q_\beta) + \frac{i\hbar}{2\sigma^2}(q-q_\beta)^2 + \gamma\right]\right\}, \tag{2}$$

where $\sigma \in \mathbb{R}$ and is proportional to the spread of the Gaussian, $\xi \in \mathbb{R}$ and is equal to the central momentum, and $\gamma \in \mathbb{R}$ and is an initial phase of the state.

Instead of the full semiclassical propagator, we apply the cubically approximated semiclassical (c.s.c.) propagator, $G^{\mathrm{csc}}(q,q',t) \propto \sum_{\mathrm{paths}} \exp\left[\frac{i}{\hbar} S^{\mathrm{cub}}(q,q',t)\right]$, to the initial state Ψ_β, giving

$$\Psi_\beta^{\mathrm{csc}}(q,t) = \int dq' G^{\mathrm{csc}}(q,q',t)\Psi_\beta(q',0). \tag{3}$$

Here we have expanded the action $S(q,q')$ up to third order around an initial position q_0 and its time evolute q_t to produce

$$\begin{aligned} S^{\mathrm{cub}}(q,q',t) = {} & S(q_t,q_0) + \left(\frac{\partial S}{\partial q_t}\right)_{q_0} Q + \left(\frac{\partial S}{\partial q_0}\right)_{q_t} Q' + \frac{1}{2}\left(\frac{\partial^2 S}{\partial q_t^2}\right)_{q_0} Q^2 + \frac{1}{2}\left(\frac{\partial^2 S}{\partial q_0^2}\right)_{q_t} Q'^2 + \left(\frac{\partial^2 S}{\partial q_0 \partial q_t}\right) Q'Q + \frac{1}{6}\left(\frac{\partial^3 S}{\partial q_0^3}\right)_{q_t} Q'^3 \\ & + \frac{1}{6}\left(\frac{\partial^3 S}{\partial q_t^3}\right)_{q_0} Q^3 + \frac{1}{2}\left(\frac{\partial^3 S}{\partial q_0^2 \partial q_t}\right) Q'^2 Q + \frac{1}{2}\left(\frac{\partial^3 S}{\partial q_0 \partial q_t^2}\right) Q' Q^2, \end{aligned} \tag{4}$$

where $Q = q - q_t$ and $Q' = q' - q_0$. This is the main extension over the harmonically approximated semiclassical (h.s.c.) propagator, and as we shall see in the following, the resulting formalism builds upon it.

Substituting the expanded action into Eq. (3) yields

$$\begin{aligned} \Psi_\beta^{\mathrm{csc}}(q,t) = {} & \sqrt[4]{\frac{1}{\pi\sigma^2}} \frac{1}{\sqrt{2\pi i\hbar}} \sum_{\mathrm{paths}} \int_{-\infty}^{\infty} dQ' \left[\left(\sqrt{\frac{\partial^2 S}{\partial Q' \partial Q}}\right)_{Q'=Q=0} + \left(\frac{\frac{\partial^3 S}{\partial Q'^2 \partial Q}}{\sqrt{\frac{\partial^2 S}{\partial Q' \partial Q}}}\right)_{Q'=Q=0} Q' + \left(\frac{\frac{\partial^3 S}{\partial Q' \partial Q^2}}{\sqrt{\frac{\partial^2 S}{\partial Q' \partial Q}}}\right)_{Q'=Q=0} Q \right] \\ & \times \exp\left\{\frac{i}{\hbar}[\Xi Q'^3 + \Upsilon Q'^2 + \Omega Q' + \Lambda]\right\}, \end{aligned} \tag{5}$$

where

$$\Xi = \frac{1}{6}\left(\frac{\partial^3 S}{\partial q_0^3}\right)_{q_t}, \tag{6}$$

$$\Upsilon = \frac{1}{2}\left[\left(\frac{\partial^2 S}{\partial q_0^2}\right)_{q_t} + \left(\frac{\partial^3 S}{\partial q_0^2 \partial q_t}\right) Q\right] + \frac{i\hbar}{2\sigma^2}, \tag{7}$$

$$\Omega = \left(\frac{\partial S}{\partial q_0}\right)_{q_t} + \left(\frac{\partial^2 S}{\partial q_0 \partial q_t}\right) Q + \frac{1}{2}\left(\frac{\partial^3 S}{\partial q_0 \partial q_t^2}\right) Q^2 + \frac{i\hbar}{\sigma^2}(q_0 - q_\beta) + \xi, \tag{8}$$

and

$$\Lambda = S(q_t,q_0) + \left(\frac{\partial S}{\partial q_t}\right)_{q_0} Q + \frac{1}{2}\left(\frac{\partial^2 S}{\partial q_t^2}\right)_{q_0} Q^2 + \frac{1}{6}\left(\frac{\partial^3 S}{\partial q_t^3}\right)_{q_0} Q^3 + \frac{i\hbar}{2\sigma^2}(q_0 - q_\beta)^2 + \xi(q_0 - q_\beta) + \gamma. \tag{9}$$

Above we have also expanded the prefactor to the next higher order around $q' = q_0$ and $q = q_t$ compared to the h.s.c. propagator; the h.s.c. propagator contains only the first term in this prefactor. However, note that the square root of the prefactor is not an entire function and so the region of convergence of any expansion is limited by where its argument is zero. As we shall see, this means that when our point of expansion is close to the zero of the argument, the overall expansion is no longer well behaved.

We let the phase in Eq. (5) be $f(Q',t)$ and the prefactor $g(Q',t)$ and then rewrite the former to fit the Airy function's cubic integral identity such that

$$\Psi_\beta^{\mathrm{csc}}(q,t) = \sum_{\text{paths}} \int dQ' g(Q',t) \exp\left\{\frac{1}{\hbar} f(Q',t)\right\}, \tag{10}$$

where

$$f(Q',t) = i(\Xi Q'^3 + \Upsilon Q'^2 + \Omega Q' + \Lambda) \tag{11}$$

$$= \Xi i\left(Q'^3 + \frac{\Upsilon}{\Xi} Q'^2 + \frac{\Omega}{\Xi} Q' + \frac{\Lambda}{\Xi}\right) \tag{12}$$

$$= \Xi i\left[\left(Q' + \frac{1}{3}\frac{\Upsilon}{\Xi}\right)^3 - \frac{1}{3}\left(\frac{\Upsilon}{\Xi}\right)^2 Q' - \frac{1}{27}\left(\frac{\Upsilon}{\Xi}\right)^3 + \frac{\Omega}{\Xi} Q' + \frac{\Lambda}{\Xi}\right] \tag{13}$$

$$= \Xi i\left[\left(Q' + \frac{1}{3}\frac{\Upsilon}{\Xi}\right)^3 - \frac{1}{27}\left(\frac{\Upsilon}{\Xi}\right)^3 + \frac{\Lambda}{\Xi} + \left(\frac{\Omega}{\Xi} - \frac{1}{3}\left(\frac{\Upsilon}{\Xi}\right)^2\right)\left(Q' + \frac{1}{3}\frac{\Upsilon}{\Xi}\right) - \frac{1}{3}\frac{\Upsilon}{\Xi}\left(\frac{\Omega}{\Xi} - \frac{1}{3}\left(\frac{\Upsilon}{\Xi}\right)^2\right)\right], \tag{14}$$

and

$$g(Q',t) = \sqrt[4]{\frac{1}{\pi\sigma^2}} \frac{1}{\sqrt{2\pi i\hbar}} \left[\left(\sqrt{\frac{\partial^2 S}{\partial Q' \partial Q}}\right)_{Q'=Q=0} + \left(\frac{\frac{\partial^3 S}{\partial Q'^2 \partial Q}}{\sqrt{\frac{\partial^2 S}{\partial Q' \partial Q}}}\right)_{Q'=Q=0} Q' + \left(\frac{\frac{\partial^3 S}{\partial Q' \partial Q^2}}{\sqrt{\frac{\partial^2 S}{\partial Q' \partial Q}}}\right)_{Q'=Q=0} Q\right]. \tag{15}$$

Thus, setting $z = -i\sqrt[3]{\frac{3}{\Xi^2}}(\Xi Q' + \frac{1}{3}\Upsilon)$ simplifies the phase such that

$$f = \frac{z^3}{3} - \zeta z + A, \tag{16}$$

where

$$\zeta = \sqrt[3]{\frac{\Xi^2}{3}}\left[\frac{\Omega}{\Xi} - \frac{1}{3}\left(\frac{\Upsilon}{\Xi}\right)^2\right], \tag{17}$$

and

$$A = i\left\{-\frac{1}{3}\Upsilon\left[\frac{\Omega}{\Xi} - \frac{1}{3}\left(\frac{\Upsilon}{\Xi}\right)^2\right] - \frac{1}{27}\frac{\Upsilon^3}{\Xi^2} + \Lambda\right\}. \tag{18}$$

Substituting in z changes the contour integral:

$$\Psi_\beta^{\mathrm{csc}}(q,t) = \sum_{\text{paths}} \int_{-i\sqrt[3]{\frac{3}{\Xi^2}}(-\Xi\infty + \frac{1}{3}\Upsilon)}^{-i\sqrt[3]{\frac{3}{\Xi^2}}(\Xi\infty + \frac{1}{3}\Upsilon)} dz\, g\big[Q'(z),t\big]\frac{dQ'}{dz} \exp\left[\frac{1}{\hbar}\left(\frac{z^3}{3} - \zeta z + A\right)\right]. \tag{19}$$

This is a convergent integral when $\frac{\pi}{6} < \arg(z) < \frac{\pi}{2}$, $\frac{5\pi}{6} < \arg(z) < \frac{7\pi}{6}$, or $\frac{3\pi}{2} < \arg(z) < \frac{11\pi}{6}$ as $|z| \to \infty$. These conditions are satisfied since $\Xi \in \mathbb{R}$ and $\Im\Upsilon = \frac{\hbar}{2\sigma^2} > 0$. Depending on the root of $\Xi^{-\frac{2}{3}}$, the possible contours of integration are equivalent to C_1 from $\infty e^{-\frac{1}{3}\pi i}$ to $\infty e^{\frac{1}{3}\pi i}$, C_2 from $\infty e^{\frac{1}{3}\pi i}$ to $\infty e^{\pi i}$, and C_3 from $\infty e^{\pi i}$ to $\infty e^{-\frac{1}{3}\pi i}$.

Thus, the integrals we must consider are

$$F(\zeta,\hbar,C_j) = \frac{1}{2\pi i}\int_{C_j} dz \exp\left[\frac{1}{\hbar}\left(\frac{z^3}{3} - \zeta z\right)\right], \tag{20}$$

$$G(\zeta,\hbar,C_j) = \frac{1}{2\pi i}\int_{C_j} dz\, z \exp\left[\frac{1}{\hbar}\left(\frac{z^3}{3} - \zeta z\right)\right]. \tag{21}$$

The contours of integration ensure that each $F(C_j)$ and $G(C_j)$ is linearly dependent on the other two [25] such that

$$F(\zeta,\hbar,C_1) + F(\zeta,\hbar,C_2) + F(\zeta,\hbar,C_3) = 0, \tag{22}$$

and the same with G.

Furthermore,

$$F(\zeta,\hbar,C_2) = \exp\left(\tfrac{2}{3}\pi i\right)F\left(\zeta e^{\frac{2}{3}\pi i},\hbar,C_1\right), \tag{23}$$

$$G(\zeta,\hbar,C_2) = \exp\left(\tfrac{4}{3}\pi i\right)G\left(\zeta e^{\frac{2}{3}\pi i},\hbar,C_1\right), \tag{24}$$

and

$$F(\zeta,\hbar,C_3) = \exp\left(\tfrac{2}{3}\pi i\right)F\left(\zeta e^{\frac{2}{3}\pi i},\hbar,C_2\right), \tag{25}$$

$$G(\zeta,\hbar,C_3) = \exp\left(\tfrac{4}{3}\pi i\right)G\left(\zeta e^{\frac{2}{3}\pi i},\hbar,C_2\right). \tag{26}$$

With these identities, the contour integrals in Eqs. (20) and (21) can be evaluated and are

$$F(\zeta,\hbar,C_1) = \hbar^{\frac{1}{3}}\mathscr{A}\left(\frac{\zeta}{\hbar^{\frac{2}{3}}}\right), \tag{27}$$

$$G(\zeta,\hbar,C_1) = -\hbar^{\frac{2}{3}}\mathscr{A}'\left(\frac{\zeta}{\hbar^{\frac{2}{3}}}\right), \tag{28}$$

and similarly for C_2 and C_3.

In summary,

$$\Psi_\beta^{\csc}(q,t) = \sum_{\text{paths}}\int_{C_j} dz\, g[Q'(z),t]\frac{dQ'}{dz}\exp\left[\frac{1}{\hbar}\left(\frac{z^3}{3}-\zeta z + A\right)\right] \tag{29}$$

$$= \sum_{\text{paths}}\int_{C_j} dz \sqrt[4]{\frac{1}{\pi\sigma^2}}\frac{1}{\sqrt{2\pi i\hbar}}\frac{i}{\sqrt[3]{3\Xi}}\left[\left(\sqrt{\frac{\partial^2 S}{\partial Q'\partial Q}}\right)_{Q'=Q=0}\right.$$

$$\left.+\left(\frac{\frac{\partial^3 S}{\partial Q'\partial Q^2}}{\sqrt{\frac{\partial^2 S}{\partial Q'\partial Q}}}\right)_{Q'=Q=0} Q + \left(\frac{\frac{\partial^3 S}{\partial Q'^2\partial Q}}{\sqrt{\frac{\partial^2 S}{\partial Q'\partial Q}}}\right)_{Q'=Q=0}\left(\frac{i}{\sqrt[3]{3\Xi}}z - \frac{\Upsilon}{3\Xi}\right)\right]\exp\left[\frac{1}{\hbar}\left(\frac{z^3}{3}-\zeta z + A\right)\right] \tag{30}$$

$$= (2\pi i)\sum_{\text{paths}}\sqrt[4]{\frac{1}{\pi\sigma^2}}\frac{1}{\sqrt{2\pi i\hbar}}\frac{i}{\sqrt[3]{3\Xi}}\left\{\left[\left(\sqrt{\frac{\partial^2 S}{\partial Q'\partial Q}}\right)_{Q'=Q=0} + \left(\frac{\frac{\partial^3 S}{\partial Q'\partial Q^2}}{\sqrt{\frac{\partial^2 S}{\partial Q'\partial Q}}}\right)_{Q'=Q=0} Q - \frac{\Upsilon}{3\Xi}\left(\frac{\frac{\partial^3 S}{\partial Q'^2\partial Q}}{\sqrt{\frac{\partial^2 S}{\partial Q'\partial Q}}}\right)_{Q'=Q=0}\right]\right.$$

$$\left.\times F(\zeta,\hbar,C_j) + \frac{i}{\sqrt[3]{3\Xi}}\left(\frac{\frac{\partial^3 S}{\partial Q'^2\partial Q}}{\sqrt{\frac{\partial^2 S}{\partial Q'\partial Q}}}\right)_{Q'=Q=0} G(\zeta,\hbar,C_j)\right\}\exp\left(\frac{A}{\hbar}\right), \tag{31}$$

where C_j runs from $-i\sqrt[3]{\frac{3}{\Xi^2}}(\Xi\infty + \frac{1}{3}\Upsilon)$ to $-i\sqrt[3]{\frac{3}{\Xi^2}}(-\Xi\infty + \frac{1}{3}\Upsilon)$.

$F(\zeta,\hbar,C_1)\exp(\frac{A}{\hbar})$ can be written in a form that makes its Q dependence explicit:

$$\hbar^{\frac{1}{3}}\mathscr{A}\left[\hbar^{-\frac{2}{3}}(\alpha Q^2 + \beta Q + \gamma)\right]\exp[i(\delta Q^3 + \epsilon Q^2 + \zeta Q + \eta)/\hbar], \tag{32}$$

where $\beta, \gamma, \epsilon, \zeta, \eta \in \mathbb{C}$ and $\alpha, \delta \in \mathbb{I}$. (See the Appendix for their explicit form.)

In this way, it can be seen that the final solution in Eq. (31) is a linear combination of an Airy function and its derivative, with complex quadratic arguments in Q, multiplied by a Gaussian with a cubic imaginary term.

Due to the variable transformation necessary to produce the Airy function form, we found it necessary that $\Xi^2 \ll (\Omega - \Xi\Upsilon^2)$ or, more loosely, that the triple derivatives of the trajectories' action be greater than or equal to the second-order derivatives with respect to the Gaussian's dispersion σ. This ensures that the Airy functions' arguments are not too large to be numerically handled by our Airy function library [26]. This is never the case early in a wave packet's propagation when its dynamics are exactly linearizable. As a consequence, in practice, early on in the dynamics the argument for the Airy function is a large number and only later does its form become numerically usable, as numerical evaluation readily showed.

As a final point on practical implementation, in numerics it is important to watch the sign of the argument $\partial^2 S/\partial q_0\partial q_t$ of the square roots of the prefactor and ensure that the roots propagate continuously on their Riemannian surface across branch cuts. This is equivalent to adding the correct Morse index into the formulation.

III. STABILITY MATRICES AND THEIR DERIVATIVES

The double action derivatives are often most easily found in terms of the elements of the stability matrix,

$$M(t) = \begin{pmatrix} M(t)_{11} & M(t)_{12} \\ M(t)_{21} & M(t)_{22} \end{pmatrix} = \begin{pmatrix} \left(\frac{\partial p_t}{\partial p_0}\right)_{q_0} & \left(\frac{\partial p_t}{\partial q_0}\right)_{p_0} \\ \left(\frac{\partial q_t}{\partial p_0}\right)_{q_0} & \left(\frac{\partial q_t}{\partial q_0}\right)_{p_0} \end{pmatrix}. \quad (33)$$

These are more convenient since they are dependent on the initial position and momentum instead of the initial and final positions. In terms of M, the double action derivatives are

$$\left(\frac{\partial^2 S}{\partial q_0^2}\right)_{q_t} = \frac{M_{22}}{M_{21}}, \quad (34)$$

$$\frac{\partial^2 S}{\partial q_0 \partial q_t} = -\frac{1}{M_{21}}, \quad (35)$$

$$\text{and} \quad \left(\frac{\partial^2 S}{\partial q_t^2}\right)_{q_0} = \frac{M_{11}}{M_{21}}, \quad (36)$$

where we dropped the stability matrix's t argument for brevity's sake and $M(0) = \mathbb{I}_{2\times 2}$.

The stability matrix of the guiding trajectory $(q_0,q_t) = (p_t,q_t)$ obeys the symplectic equation of motion

$$\dot{M}(t) = K(t)M(t), \quad (37)$$

where

$$K(t) = \begin{pmatrix} -\frac{\partial^2 H}{\partial q \partial p} & -\frac{\partial^2 H}{\partial q^2} \\ \frac{\partial^2 H}{\partial p^2} & \frac{\partial^2 H}{\partial p \partial q} \end{pmatrix}. \quad (38)$$

Similarly, the triple derivatives of the action can often most easily be found in terms of the elements of the stability matrix and its first derivative $\Gamma(t) \equiv \frac{\partial M}{\partial(p_0,q_0)}$, a $2\times 2\times 2$ tensor. The equation of motion for $\Gamma(t)$ can be shown to be

$$\dot{\Gamma}(t)_{ilm} = \sum_{j,k} \frac{\partial K(t)}{\partial(p,q)}_{ijk} M(t)_{kl} M(t)_{jm} + \sum_j K(t)_{ij} \Gamma(t)_{jlm}, \quad (39)$$

where

$$\frac{\partial K(t)}{\partial p} = \begin{pmatrix} -\frac{\partial^3 H}{\partial q \partial p^2} & -\frac{\partial^3 H}{\partial q^2 \partial p} \\ \frac{\partial^3 H}{\partial p^3} & \frac{\partial^3 H}{\partial q \partial p^2} \end{pmatrix} \quad (40)$$

$$\text{and} \ \frac{\partial K(t)}{\partial q} = \begin{pmatrix} -\frac{\partial^3 H}{\partial q^2 \partial p} & -\frac{\partial^3 H}{\partial q^3} \\ \frac{\partial^3 H}{\partial p^2 \partial q} & \frac{\partial^3 H}{\partial q^2 \partial p} \end{pmatrix}. \quad (41)$$

In terms of the Γ tensor, the triple action derivatives are

$$\frac{\partial^3 S}{\partial q_0^3} = \frac{1}{M_{21}}\Gamma_{222} - 2\frac{M_{22}}{(M_{21})^2}\Gamma_{221} + \frac{(M_{22})^2}{(M_{21})^3}\Gamma_{211}, \quad (42)$$

$$\frac{\partial^3 S}{\partial q_0^2 \partial q_t} = \frac{1}{(M_{21})^2}\left(\Gamma_{212} - \frac{M_{22}}{M_{21}}\Gamma_{211}\right), \quad (43)$$

$$\frac{\partial^3 S}{\partial q_t^3} = \frac{1}{(M_{21})^2}\left(\Gamma_{111} - \frac{M_{11}}{M_{21}}\Gamma_{211}\right), \quad (44)$$

$$\frac{\partial^3 S}{\partial q_0 \partial q_t^2} = \frac{\Gamma_{211}}{(M_{21})^3}, \quad (45)$$

and $\Gamma(0) = 0 \times \mathbb{I}_{2\times 2\times 2}$.

In many applications there is often no need to maintain strict symplecticity or conservation of the area of phase space when calculating $\Gamma(t)$. Instead, it can be found by numerical approximation to an acceptable accuracy, such as perhaps by a finite difference evaluation from two stability matrices for two trajectories, with initial conditions slightly displaced from each other. This is especially important for applications in "on-the-fly" calculations, where the stability matrix is computed by *ab initio* methods and generally relies on an expensive calculation of the system's Hessian matrix to find $K(t)$. Thus, for instance, using a finite difference computational approach would be expected to double the amount of Hessians that must be computed. This is still a far cry from the many more that are necessary, one for each trajectory's stability matrix, in contemporary "initial-value methods" such as the Herman-Kluk propagator.

IV. PERFORMANCE OF THE CUBIC APPROXIMATION

To evaluate the performance of the cubic approximation we derived, we examine the first return of an initially displaced and kicked coherent state with $\hbar = 1$, $\sigma = 1/\sqrt{8}$, $q_\beta = 1$, and $p_\beta = -300$, under the Hamiltonian $H = \frac{p^2}{2m} + \omega|q^3|$ with $m = 1$, $\omega = 10\,000$. Although trajectories under this system's evolution have higher than triple action derivatives, the triple derivatives dominate in an interval of values for $\hbar$ (with respect to σ) that we focus on, as we will show. In this regime this potential exhibits isolated hairpins in phase space and negligible fourth- or higher-order kinks.

Figure 1 shows a few time steps after the first period of the wave packet's orbit during the time interval when it is traversing past its initial state. As can be seen, at the beginning of this interval the wave packet has nearly reformed to a Gaussian state after its collision with the near wall. It then develops oscillatory anharmonic features as it returns to the far wall. These oscillations in its absolute value are indicative of two contributing branches in q space of the wave function, as we shall see when we examine its propagation in phase space shortly. In the second column the quadratic approximation is shown capturing the center of mass of the wave packet well, but it is clearly unable to reproduce the two branches that produce the nonlinear oscillations. Compared to the quadratic's performance, the cubic approximation is able to capture these features far more successfully, as shown in the third column. This indicates that the cubic treatment can handle highly anharmonic propagation that produces significant curvature in phase space with only a single guiding trajectory. For the quadratic and cubic runs shown, the guiding trajectory (p_t,q_t) at all times was chosen to be the center of mass of the initial state at $t = 0$ and so required no root searching.

The real part of the numerically evaluated autocorrelation, $\langle\Psi_\beta(0)|\Psi_\beta(t)\rangle = \int_{-\infty}^{\infty} dq\ \Psi_\beta^*(q)\Psi_\beta(q,t)$, exhibits similar performance differences between the quadratic and cubic methods during the same time interval. As seen in Fig. 2, the quadratic expansion is able to capture the overall envelope of the first recurrence in the autocorrelation well. However, unlike the cubic approximation, it is unable to reproduce the chirp in the frequency during the recurrence as well as the variations in its envelope.

Figure 3 shows the 4.9-σ confidence interval of the initial classical Gaussian distribution and its final time evolute at the time steps indicated during the recurrence. Also shown are the

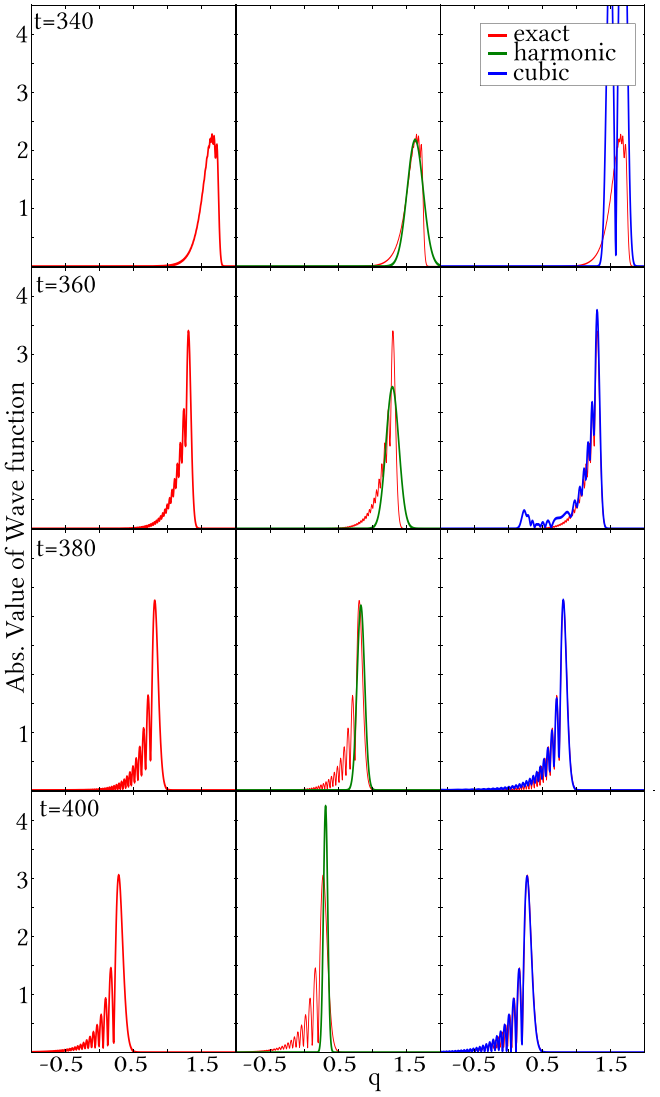

FIG. 1. The first recurrence of the wave packet with its initial coherent state in the absolute value cubic potential described inline. At $t = 340$ the wave packet has just reflected off of the right wall and is fairly Gaussian in appearance. As it proceeds back across the potential at $t = 360$ to $t = 400$, the absolute value of its wave function becomes far more asymmetric and oscillatory. The cubic approximation to this evolution, expanded around the classical guiding trajectory at the center of the wave packet, appears to be able to capture this latter behavior far better than the quadratic approximation and GGWPD.

equivalent confidence intervals generated from quadratically and cubically expanding the action around the initial and final positions of the central guiding trajectory (the latter are marked by the black x's) up to that time point. They show that at $t = 340$ only the far-off tails of the classical density have passed through the latter's initial self, while at $t = 380$ the wave packet has rotated and its central highest density is now sweeping through. Finally, at $t = 400$, the central density is seen exiting the initial 4.9-σ confidence interval.

It is clear in these snapshots of phase space that the initial spread $\sigma = 1/\sqrt{8}$ is such that the state's classical density exhibits significant curvature after its first period. Decreasing σ while keeping $\sigma/\hbar$ fixed allows the quadratic approximation

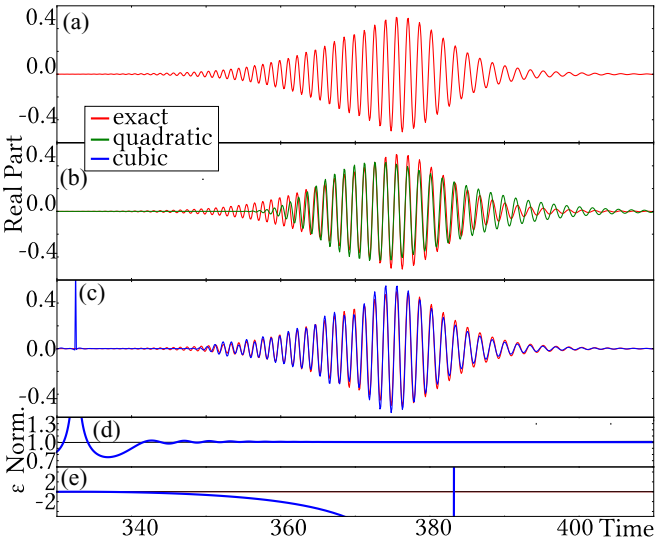

FIG. 2. The first recurrence in the autocorrelation according to (a) full quantum propagation, (b) the semiclassical quadratic and (c) cubic approximations, (d) the normalization of the cubic approximation, and (e) ϵ, which is defined in the text. These are for the coherent state and cubic potential described in text with time step $\Delta t = 8 \times 10^{-5}$. The cubic autocorrelation diverges from unit normalization immediately before the recurrence when the wave packet bounces against the near wall.

to perform better in the time period examined because less of the density in phase space is able to develop curvature, and only one branch contributes within an area of $\hbar$. Increasing σ with respect to $\hbar$ leads both the quadratic and cubic approximations to perform badly as the density becomes too stretched out. In this case, using just the central guiding trajectory is insufficient because multiple hairpins begin to overlap the initial state which require corresponding guiding trajectory. An example of how to properly handle this regime is shown in Sec. VII and generally requires root searching.

In other words, with only a single central guiding trajectory at intermediate times, the cubic approximation is expected to be superior to the quadratic one only for intermediate

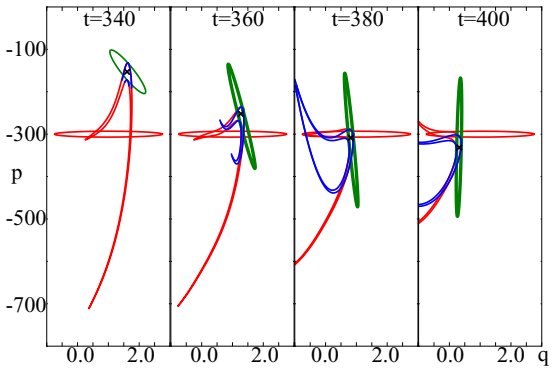

FIG. 3. The 4.9-σ confidence intervals of the initial and classically propagated final states in phase space around the time of the middle of the recurrence. Along with the full time evolution, also shown is the quadratically and cubically approximated evolution of the state around the guiding trajectory marked by "x."

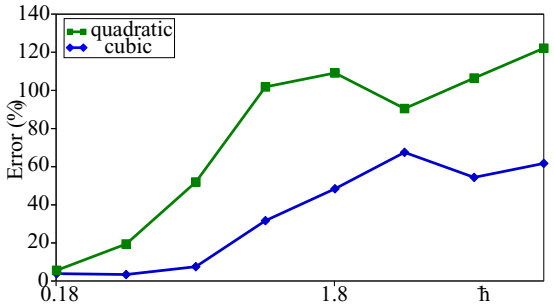

FIG. 4. The error $|C_\beta^{\text{c.s.c./h.s.c}}(t) - C_\beta(t)|/|C_\beta(t)|$ averaged over all absolute values greater than 0.01 in the time interval $t = 350$ to $t = 500$ with $\Delta t = 1$ for different values of $\hbar$. These are plotted on a logarithmic scale with $\sigma/\hbar$ kept fixed. When $\hbar = 1$, $\sigma = 1/\sqrt{8}$, which are the parameters used in the evolution under the absolute value cubic potential discussed in the text.

values of $\hbar$ when the cubic curvature of the state's manifold in phase space becomes significant. For larger values of $\hbar$, when more hairpins contribute to phase-space overlaps and higher orders of curvature become important, it is expected to only be nominally better. On the other hand, as $\hbar \to 0$ the quadratic expansion should become exact. This is confirmed in Fig. 4 where the errors of the two methods (using the same central guiding trajectory) are compared at different values of $\hbar$.

In this vein, choosing a more appropriate "off-center" guiding trajectory to better capture the phase-space overlap at each time step during the first recurrence, and more than one trajectory when multiple branches contribute, will improve both the quadratically and cubically approximated autocorrelation. However, the quadratically approximated recurrence will never be exact for large enough $\hbar$, because two very close guiding centers are necessary to treat the tip of the hairpin's contribution when it passes through its initial state in phase space. These two guiding centers will always become too close together and their respective Gaussians will overlap. The proper treatment of these two coalescing guiding centers necessitates a "uniformization"—the cubic approximation—as will be explained in the next section, Sec. V.

Further examining the behavior of the cubic approximation, it is clear that immediately before the first recurrence shown in Fig. 2 the expression is not well behaved as the wave packet hits the near wall. This can be seen in its nonunitary normalization around $t = 333$ in the second-lowest panel of Fig. 2, as well as in the peak at the same time point in its autocorrelation one panel above. This occurs for the reasons intimated in the earlier derivation, namely, due to the expansion of the prefactor, which is not an entire function. In particular, $\sqrt{\partial^2 S(q,q',t)/\partial q \partial q'}$ is discontinuous at $\partial^2 S(q,q',t)/\partial q \partial q' = 0$, and any expansion about q' and q will have its radius of convergence bounded by this value. So, it is important that this discontinuity does not fall on heavily weighted regions of the $z(q')$ domain over which the integral in Eq. (19) is performed, namely, anywhere near the initial wave packet. If this occurs, the expansion is not well behaved and the integral over $z(q')$ becomes poor. For a particular Q, the discontinuity of the prefactor in q' with respect to q_0 lies at

$$q_0' - q_0 = -\frac{\sqrt{\frac{\partial^2 S}{\partial q_0 \partial q_t}}}{\frac{\partial^3 S}{\partial q_0^2 \partial q_t}}\left[\sqrt{\frac{\partial^2 S}{\partial q_0 \partial q_t}} + \frac{\frac{\partial^3 S}{\partial q_0 \partial q_t^2}}{\sqrt{\frac{\partial^2 S}{\partial q_0 \partial q_t}}} Q\right]. \quad (46)$$

Hence, for all Q, when $\epsilon \equiv \frac{\partial^2 S}{\partial q_0 \partial q_t} / \frac{\partial^3 S}{\partial q_0^2 \partial q_t} = 0$ the discontinuity lies directly on q_0—the initial position of the guiding trajectory. For the example we have shown so far, this corresponds to the center of the initial wave packet. We show in last panel of Fig. 2 that this is exactly what happens at $t = 333$ (and at later turning points) and is the reason for the violation of the expression's unitarity. Namely, at turning points, $\partial^2 S/\partial q_0 \partial q_t = \partial p_t/\partial q_0 \to 0$ and so $\epsilon \to 0$. Hence, for centered guiding trajectories, the discontinuity of the square root causes the most important part of phase space to be poorly approximated during turning points. This issue can be mitigated most simply by choosing a different, perhaps nearby, guiding trajectory, which is not near a turning point at the troublesome time steps.

As we have made clear so far, the quadratically and cubically approximated calculations both rely on one or more real guiding trajectories at each time step to approximate the dynamics of nearby phase space. It can be easily shown that the quadratically approximated evolution of the classical density is equivalent to expanding the potential around the guiding trajectory up to second order at every time step [17]. This means that the classical density remains real at all times and maintains its Gaussian form in its position-space projection. This is clear in Fig. 3 by its conserved elliptically shaped confidence interval. On the other hand, the cubically approximated evolution of the classical density by the expansion of its action around the initial q' and final q is not equivalent to expanding the potential around the guiding trajectory up to third order. In particular, it is easy to show that cubic potentials have infinite orders of powers of initial q' and final q in their action.

Perhaps a surprising consequence of this last statement is that the cubically approximated classical density does not necessarily remain real. In particular, since we expand our action up to third order in q' and q, it follows that

$$-p' = \frac{\partial S}{\partial q'} = \frac{\partial S}{\partial q_0} + \frac{\partial^2 S}{\partial q_0^2} Q' + \frac{\partial^2 S}{\partial q_0 \partial q_t} Q + \frac{1}{2}\frac{\partial^3 S}{\partial q_0^3} Q'^2 + \frac{\partial^3 S}{\partial q_0^2 \partial q_t} Q' Q + \frac{1}{2}\frac{\partial^3 S}{\partial q_0 \partial q_t^2} Q^2 \quad (47)$$

and

$$p = \frac{\partial S}{\partial q} = \frac{\partial S}{\partial q_t} + \frac{\partial^2 S}{\partial q_t^2} Q + \frac{\partial^2 S}{\partial q_0 \partial q_t} Q' + \frac{1}{2}\frac{\partial^3 S}{\partial q_t^3} Q^2 + \frac{\partial^3 S}{\partial q_0 \partial q_t^2} Q' Q + \frac{1}{2}\frac{\partial^3 S}{\partial q_0^2 \partial q_t} Q'^2, \quad (48)$$

where p' and p are the initial and final momenta of the trajectory (q',q), and $Q' = q' - q_0$ and $Q = q - q_t$ again. It follows that the final position with respect to q_t is

$$Q = \frac{1}{2a}(-b \pm \sqrt{b^2 - 4ac}), \quad (49)$$

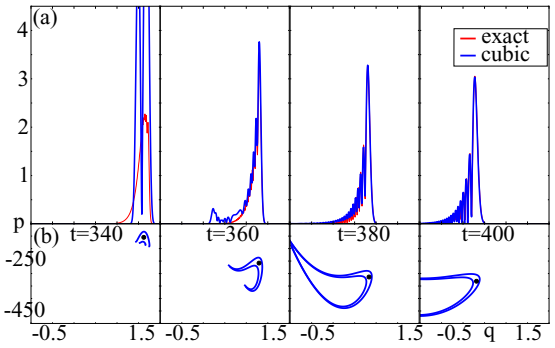

FIG. 5. (a) The cubically approximated wave function from Fig. 1 and (b) the cubically approximated dynamics of the classical density that are real from Fig. 3. As described in the text, the abrupt terminations of the purely real parts of the classical density at time steps 340 and 360 produce the two lobes seen in the wave packet.

where

$$a = \frac{1}{2}\frac{\partial^3 S}{\partial q_0 \partial q_t}, \tag{50}$$

$$b = \frac{\partial^2 S}{\partial q_0 \partial q_t} + \frac{\partial^3 S}{\partial q_0^2 \partial q_t}(q' - q_0), \tag{51}$$

and

$$c = \frac{\partial S}{\partial q_0} + \frac{\partial^2 S}{\partial q_0^2}(q' - q_0) + \frac{1}{2}\frac{\partial^3 S}{\partial q_0^3}(q' - q_0)^2 + p'. \tag{52}$$

Hence, $|\Im q_t| > 0$ when the discriminant $b^2 - 4ac$ is negative. This condition is satisfied at times for the parts of the classical density during the time interval shown and so leads them to become complex valued.

We showed the 4.9-σ confidence intervals of the cubically approximated density, restricted to the trajectories with no imaginary part, in Fig. 3 (in blue). For convenience, these fragments are replotted without the other curves in Fig. 5 below their corresponding wave packets in position representation. At $t = 340$ and $t = 360$, the real parts of the cubically evolved classical densities are shown abruptly terminating at two regions, after which they are complex. These correspond to the boundary in phase space where the discriminant becomes negative. At $t = 380$ and $t = 400$ the entire classical density within the confidence interval shown becomes real again.

Since the cubically approximated expression involves an integral over all real q' and q, the abrupt transitions of the classical density to complex space has the effect of discontinuously changing the integral's domain, since the trajectories whose positions become complex are not included in the integral. In particular, the two lobes of the wave packet at $t = 340$ correspond to the q projection of the two abrupt terminations of the classical density shown below. These two lobes become the two larger ripples along the wave packet at $t = 360$. They are smaller in amplitude since fewer of the classical trajectories have become complex, as can be seen in the thinner ends of the "legs" in the phase-space confidence intervals at $t = 360$.

It is unclear whether this feature has a physical interpretation concerning the dynamics. Regardless, the cubic approximation to the wave packet evolution fares poorer when significant portions of the corresponding real initial classical density have become complex valued. In practice, we found that the intervals of time when this occurs are relatively short, and even when they occur, the resultant wave packets are still often superior to the quadratic approximation. The cubically approximated wave packet at $t = 360$, for example, is still far closer to the exact one compared with the quadratic approximation, despite its two anomalous peaks.

V. METHOD OF STEEPEST DESCENTS

An alternative quadratic evaluation of

$$\Psi_\beta(q,t) = \int dq' G^{\text{vVMG}}(q,q',t)\Psi_\beta(q',0) \tag{53}$$

is by the method of steepest descents [27–30]. This is equivalent to the quadratic approximation already presented, except that the guiding centers around which the expansion is made become the saddle points of the integrand—the initial and final positions where the first derivative of the phase is equal to zero. Such a treatment is on a more formally solid footing compared to the previous approach, since these guiding trajectories are well defined. However, the resultant guiding trajectories are often complex valued and need to be found by root-finding methods. More precisely, the expansion of the action in Eq. (4) is made around the saddle points in phase space of the integrand, which are generally complex trajectories (p_t,q_t), obeying double-ended boundary conditions. The result, which is the mixed coherent state and position representation of the time-dependent WKB approximation and also the position representation of GGWPD, is

$$\begin{aligned}\Psi_\beta(q,t) &= \sqrt[4]{\frac{1}{\pi\sigma^2}} \sum_{\text{saddle points}} \sqrt{\frac{-\partial^2 S/\partial q_0 \partial q}{\left(\partial^2 S/\partial q_0^2\right)_{q_t} + i\hbar/\sigma^2}} \\ &\times \exp\left[\frac{i}{\hbar}S(q,q_0,t)\right] \exp\left[\frac{i\sigma^2}{\hbar^2}\Re p_0 \Im p_0 - \frac{\sigma^2}{2\hbar^2}(\Im p_0)^2 \right. \\ &\left. - \frac{1}{2\sigma^2}(\Im q_0)^2 - \frac{1}{\hbar}\Re p_0 \Im q_0\right],\end{aligned} \tag{54}$$

where the sum is over all saddle points (guiding trajectories) that satisfy

$$0 = \frac{1}{\sigma^2}(q_0 - q_\beta) + \frac{i}{\hbar}(p_0 - p_\beta) \tag{55}$$

and

$$q_t = q. \tag{56}$$

Unlike for the real-trajectory methods explored before, these two equations define specific conditions that the guiding trajectories $(p_0,q_0) \to (p_t,q_t)$ must satisfy. For this to be possible, in general $(p_0,q_0) \in \mathbb{C}^2$ while $(p_t,q_t) \in \mathbb{R}^2$ and so the guiding trajectories cannot begin by being real.

The performance of the steepest descents method applied to the prior absolute cubic potential is shown in the right column of Fig. 6. There it is clear that the GGWPD wave packet agrees closely with the exact evolution and captures

the interference oscillations very well. This is accomplished by including two saddle-point contributions in the sum of Eq. (54) corresponding to the two branches on the left side of the hairpin. These are marked as black dots in the phase-space plots in the left column of Fig. 6. On the right side of the hairpin, two saddle points can still be found very close to each other, though only one is expected. However, the lower of the two appears to have traversed a Stokes line and contributes anomalously large amplitude. Therefore, we only include the upper saddle point contribution. Even so, at the last two time steps ($t = 380$ and $t = 400$), the tight hairpin becomes so tight perpendicular to its q projection that the saddle points on the two branches at and after the hairpin coalesce too closely to each other (with respect to $\hbar$) vertically. This leads to the formation of the anomalous peak at the right side of the GGWPD wave packet where the method of steepest descents fails, even when only keeping the top branch of saddle points. Notice that at $t = 400$ these two branches to the right of the hairpin have fused into one branch. This suggests a relationship between saddle points crossing a Stokes line and the coalescence of two branches. However, we do not pursue this subject further in this paper.

We point out the relatively large amount of work necessary to produce this GGWPD result: at every q the correct two saddle points had to be found by root searching through the four-dimensional complex space corresponding to complex classical trajectories. The cubic approximation, on the other hand, is able to capture both of the contributions caused by the curvature automatically from only one guiding trajectory, and so reproduces most of the interfering features with no additional work for different qs.

The quadratic real-trajectory or "thawed Gaussian approximation" has been recently argued to be an approximation to GGWPD in that it approximates the latter's complex

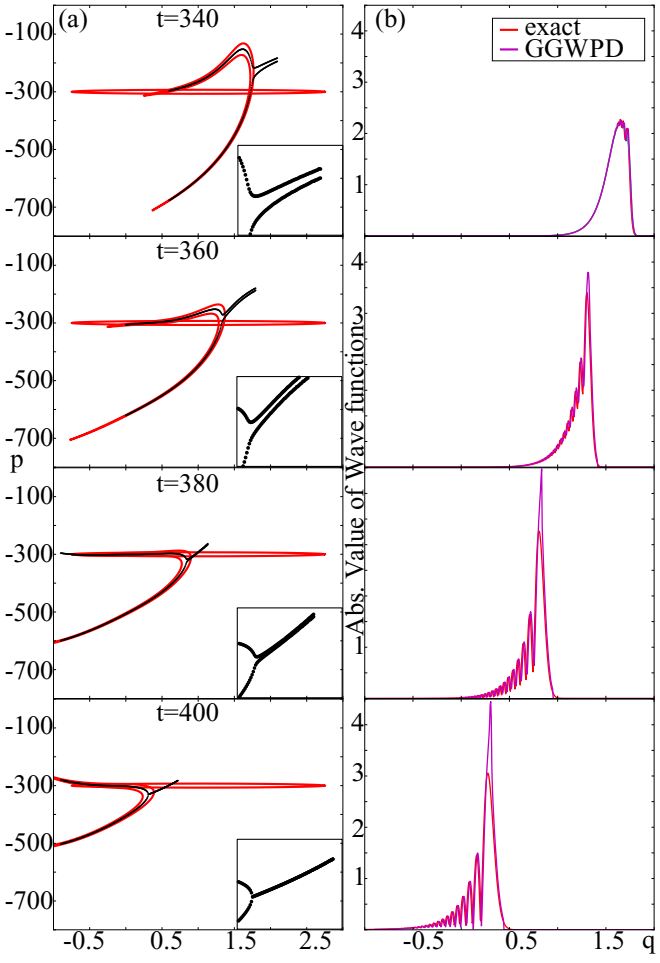

FIG. 6. (a) The 4.9-σ confidence intervals of the classical densities alongside their (b) corresponding exact and GGWPD-generated wave packets at four time points. Also shown are the real parts of the complex guiding trajectories (p_t, q_t) (marked as black dots, with their area of coalescence magnified in the inset) used to produce the wave packet at every q value. A pair of guiding trajectory contributions, each from one of the two branches, was included for the part of the quadratic wave packet to the left of the hairpin. The part to the right was constructed by only including the upper branch.

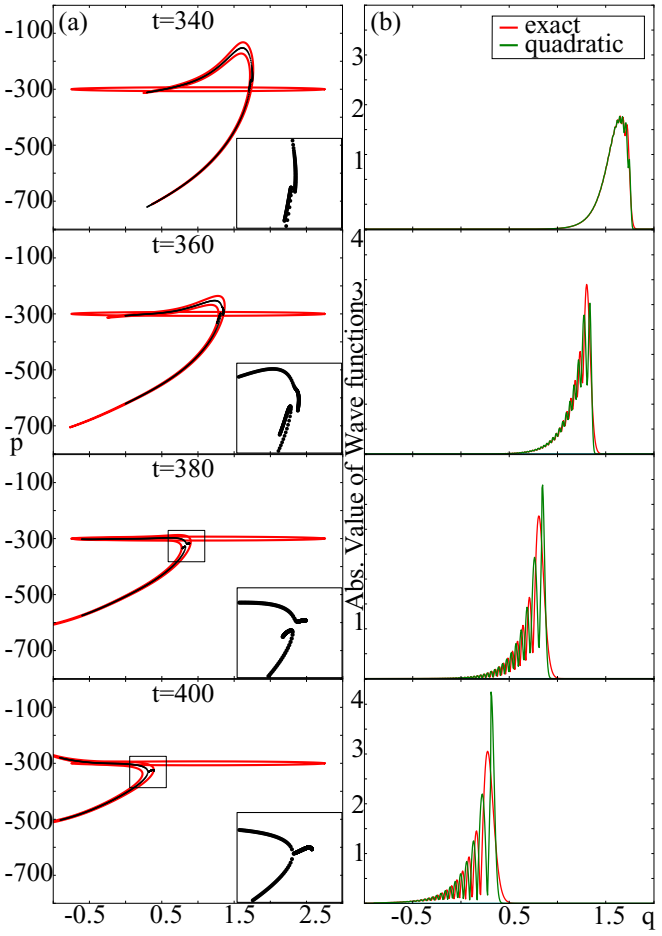

FIG. 7. The (a) 4.9-σ confidence intervals from Fig. 6 and the final real "off-center" guiding trajectories (p_t, q_t) (marked as black dots, with their area of coalescence magnified in the inset). (b) The quadratic approximation to the wave packets at every q value produced from these guiding trajectories. Like in the GGWPD case, a pair of guiding trajectory contributions, each from one of the two branches, was included for the part of the quadratic wave packet to the left of the hairpin. The part to the right was constructed by including only the upper branch. The initial values of the real trajectories were chosen to be the real parts of the initial complex saddle-point trajectories used in GGWPD in Fig. 6.

trajectories by their closest corresponding real trajectories [31]. In other words, the guiding trajectories in the quadratic approximation can be considered to be real-trajectory analogs to the original integrand's complex saddle-point trajectories, which define the more formal GGWPD.

To explore this relationship, we used the real parts of the initial complex saddle-point trajectories found at every q value in GGWPD as the guiding trajectories for the quadratic real-trajectory approximation. As shown in Fig. 7, their time evolutes lie along the center of the two branches of the confidence interval in phase space to the left of the hairpin, just like the real parts of the evolved complex trajectories shown in Fig. 6 do. However, to the right of the hairpin this relationship is broken and the lower real trajectories curve left while the rest go right. The latter's contributions were kept while the former's were discarded to produce the wave packets in Fig. 7, just like we discarded the lower branch when we looked at the GGWPD. However, unlike that case, the reasons for not keeping them are perhaps more obvious in the real-trajectory case; the real guiding trajectories that capture the part of the wave packet to the right of the hairpin should also lie to the right. Finally, after $t = 380$ the two branches fuse to become one, as was also seen in GGWPD.

Notice that the quadratic real-trajectory evaluation in Fig. 7 is just as accurate as GGWPD away from the hairpin. Around the hairpin it fails due to the two Gaussians corresponding to its two guiding trajectories beginning to overlap. This is the real-trajectory manifestation of coalescing saddle points and causes the approximation to fail faster than the GGWPD's failure of the method of steepest descents. The cubic approximation derived here is a uniformization of this quadratic real-trajectory method and handles these two overlapping Gaussians. It works so well in the example shown so far, in fact, that using only one guiding trajectory for every q seems largely sufficient.

As an aside, it is possible to formulate a superior steepest descents equivalent to the cubic approximation presented here, in the same way that GGWPD is the superior steepest descents equivalent of the real-trajectory quadratic approximation. Such a formulation would also be a "uniformization" in that it would properly handle two (or more) coalescing saddle phase-space points, which are the marker of phase-space curvature, in a uniform manner. Indeed, the derivation would follow the same steps as those laid out here but with the phase $f(Q',t)$ expanded around its saddle points. Again, the cubic approximation presented here could be interpreted as a real-trajectory approximation to such a uniform steepest descents treatment, the latter of which would instead generally involve complex trajectory root finding of what would now be pairs of complex trajectories.

Returning back to GGWPD, we proceed to examine its evaluation of the autocorrelation during the first recurrence by performing the integral in Eq. (54) with another coherent state by the method of steepest descents. This is in contrast to the numerical evaluation of the integral and allows us to consider only the neighborhoods near the set of saddle-point trajectories that satisfy the new steepest descent conditions. Numerical integration with a coherent state, which is what we examined for the quadratic and cubic approximations to the autocorrelation, is comparably difficult to perform with the position representation of GGWPD due to the necessity of finding the correct roots for every q point at every time step. Its evaluation by the method of steepest descents produces the coherent state representation of time-dependent WKB, or the coherent state representation of GGWPD, and is

$$\begin{aligned}\langle\Psi_\beta|\Psi_\beta(t)\rangle = {} & \frac{1}{\sqrt{2i\hbar\sigma}} \sum_{\text{saddle points}} \exp\left(\frac{i}{\hbar}S(q_t,q_0,t)\right)\sqrt{\frac{-\partial^2 S/\partial q_0\partial q_t}{\left[1/2\sigma^2 - i\left(\partial^2 S/\partial q_t^2\right)_{q_0}/2\hbar\right]\left[1/2\sigma^2 - i\left(\partial^2 S/\partial q_0^2\right)_{q_t}/2\hbar\right] + \frac{1}{4\hbar^2}\left[\frac{\partial^2 S}{\partial q_t\partial q_0}\right]^2}} \\ & \times \exp\left[\frac{i\sigma^2}{\hbar^2}\Re p_0\Im p_0 - \frac{\sigma^2}{2\hbar^2}(\Im p_0)^2 - \frac{1}{2\sigma^2}(\Im q_0)^2 - \frac{1}{\hbar}\Re p_0\Im q_0\right] \\ & \times \exp\left[\frac{i\sigma^2}{\hbar^2}\Re p_t\Im p_t - \frac{\sigma^2}{2\hbar^2}(\Im p_t)^2 - \frac{1}{2\sigma^2}(\Im q_t)^2 + \frac{1}{\hbar}\Re p_t\Im q_t\right],\end{aligned} \tag{57}$$

where now the sum is over all saddle points that satisfy

$$0 = \frac{1}{\sigma^2}(q_0 - q_\beta) + \frac{i}{\hbar}(p_0 - p_\beta) \tag{58}$$

and

$$0 = \frac{1}{\sigma^2}(q_t - q_\beta) - \frac{i}{\hbar}(p_t - p_\beta), \tag{59}$$

for (p_0,q_0) and $(p_t,q_t) \in \mathbb{C}^2$. Again, the guiding trajectories $(p_0,q_0) \to (p_t,q_t)$ must satisfy these two conditions and so are generally complex valued.

Figure 8 shows that GGWPD is able to capture the first recurrence in the autocorrelation very well. Its only apparent deviation from the exact curve can be found in its amplitude, which is slightly too low in the middle. We attribute this underestimation of the amplitude to the fact that we only included one saddle-point contribution in the sum this time around. A search in nearby complex phase space reveals another saddle point where it is expected, shown in the bottom panel of Fig. 8 where it is the leftmost black dot. Promisingly, it was found to contribute negligible amplitude before $t = 360$ and then significantly larger amplitude during the middle of the recurrence, as desired. Unfortunately, this contribution is badly behaved and is increasingly too large in magnitude. For this reason it was not included. It is not clear whether this is due to that saddle point traversing a Stokes line or if it is a valid contribution and its bad behavior is due to the coalescence together of these two saddle points. As we have seen, these two phenomena appear to be related. Regardless, it is not

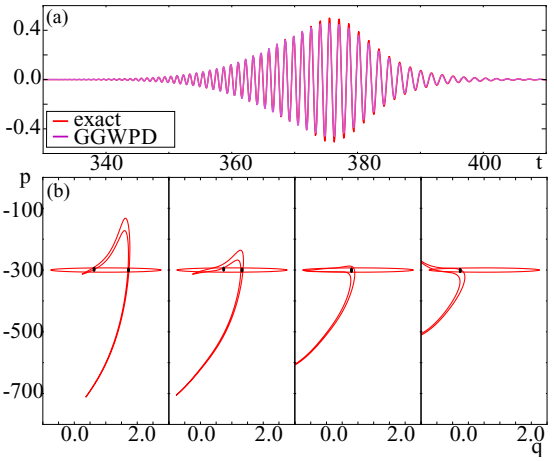

FIG. 8. (a) The real part of the GGWPD autocorrelation is compared to the exact first recurrence. Notice the underestimation of the exact amplitude by GGWPD in the middle of the recurrence. (b) The 4.9-σ confidence intervals are shown along with the two saddle-point trajectories drawn as black dots for the coherent state representation of the GGWPD. These saddle points appear to coalesce together around $t = 380$.

surprising that GGWPD fails to be exact in the middle of the recurrence, since it should require at least two saddle points to capture the recurrence, which judging from the phase-space confidence intervals at $t = 380$ will be very close together.

VI. GUIDING TRAJECTORIES

The quadratic approximation's accuracy has often been found to be relatively insensitive to the selection of an appropriate real guiding trajectory. In fact, many results [12,32] have been obtained using only the central trajectory of the initial coherent state as the guiding trajectory, as we also did for the results shown in Figs. 1 and 2. However, when the dynamics of the state become more anharmonic, the selection of an "off-center" guiding trajectory becomes more important.

To explore the cubic approximation's sensitivity to the appropriate guiding trajectory, we examine its performance of the autocorrelation during the four times indicated in Fig. 1 under different guiding trajectories. To see this, we show the overlap in phase space of the classical density corresponding to the wave packet with its initial self in Fig. 9. Its 4.9-σ confidence intervals are drawn in red in both columns over the underlying contour plots. The contour plots show the error in approximating the recurrence from using the corresponding guiding trajectories. The shading corresponds to the error in the first recurrence of the wave packet propagated by a guiding trajectory that ends at the phase-space point (p_t,q_t) indicated by the abscissas and ordinates. The lighter the shading, the greater the error, or equivalently, the poorer the corresponding guiding trajectory (p_t,q_t) fares at capturing the overlap at the time step shown. The left column shows the error from the quadratic expansion at the guiding trajectories while the right column shows the cubic expansion's error.

As expected, the region of good candidate guiding trajectories (p_t,q_t) is quite consistently broad for the quadratic approximation and seems to itself be fairly Gaussian in shape.

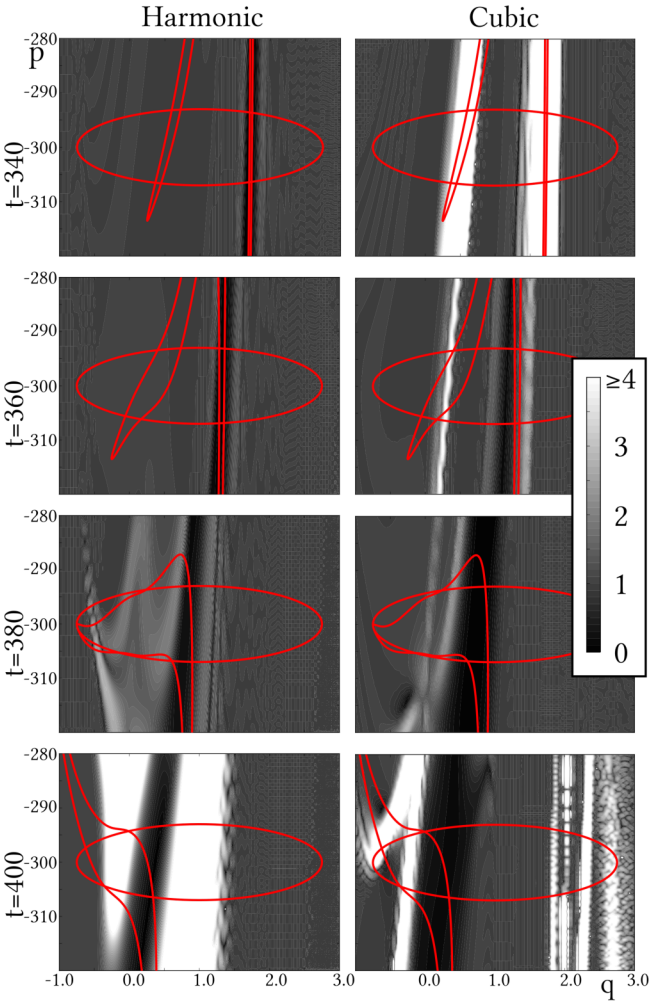

FIG. 9. Error, $\frac{|C_\beta^{\mathrm{hsc/csc}}(t)-C_\beta(t)|}{|C_\beta(t)|}$, for guiding trajectories (p_t,q_t) ending at the phase-space point indicated by the axes for the time interval shown in Fig. 2. Darker regions correspond to guiding trajectories that lead to the most accurate approximation of the overlap, while lighter regions correspond to poorer trajectories. As can be seen in this side-by-side comparison between the quadratic and cubic approximations, while the area of acceptable phase space from which the quadratic approximation's guiding center can be selected is quite consistent and appears almost Gaussian shaped itself, it is significantly more variable for the cubic case. In particular, the cubic approximation's valid guiding center area is smallest when it is least applicable immediately after a turning point and is largest when the third-order action derivatives dominate over all others.

However, selecting a better guiding trajectory than the center of the wave packet from these darker phase-space regions does greatly improve the quadratic approximation's autocorrelation for the first half of the recurrence shown in Fig. 2, a procedure that is largely unnecessary for the cubic approximation since it fares just fine with the central guiding trajectory.

On the other hand, the cubic approximation's region of good candidate trajectories (p_t,q_t), indicated by its growing black area, appears to be highly variable in shape and size. At $t = 340$ the cubic approximation is still suffering the last effects of its bad behavior at the preceding caustic and has only a very thin black region around $q = 1.3$. This region

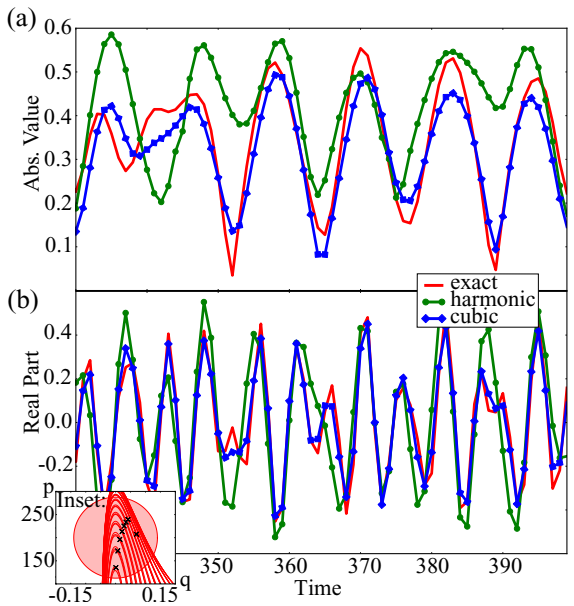

FIG. 10. The (a) absolute value and (b) real part of the autocorrelation of an initial coherent state with $\sigma = 0.057$, $q_\beta = 0$, $p_\beta = 200$ in the Morse potential $H = \frac{p^2}{2m} + D[1 - \exp(-\alpha q)]^2$ with $m = 1$, $D = 50\,000$, $\alpha = 8$ and with time step $\Delta t = 0.000\,05$. The cubic expansion is able to capture the local nonlinearity in the autocorrelation. (Inset: The collection of periodic orbits shown in phase space which additively contribute to the semiclassical wave packet [the sums over paths in Eq. (31) at $t = 350$.)

grows substantially with time, dwarfing the corresponding quadratic approximation's black area during the time span when the cubic approximation is seen to most closely approach the exact propagation in Fig. 1. This suggests that when the cubic approximation is performing best, it is more insensitive to "incorrect" guiding trajectories compared to the quadratic approximation, and vice versa.

VII. SUM OVER INDIVIDUAL CONTRIBUTIONS

As time increases, growing numbers of periodic or heteroclinic orbits usually intersect with an area in phase space. Adding all of them with appropriate phases, from a manifold of guiding trajectories, is necessary to approximate the full wave packet's auto- or crosscorrelations. As discussed in detail in Sec. V, the "Method of Steepest Descents," this sum is the real-trajectory equivalent to the saddle-point sum formally present in the coherent state representation of GGWPD in Eq. (57). The quadratically expanded propagator has been shown to handle this properly, as mentioned before in the cases of the Coulombic potential and the stadium billiard. However, when these individual contributions are highly curved themselves such that they must be captured by pairs of saddle points in GGWPD (and appear as hairpins in phase space), the quadratic approximation struggles. This is clear in Fig. 10, which shows the autocorrelation at some time interval for an initial coherent state evolving under a Morse potential—often used to realistically model the anharmonicity in molecular vibrational bonds—whose parameters can be found in the caption. Figure 10(a) shows the absolute value of the autocorrelation, while Fig. 10(b) shows the real part. The inset shows the confidence intervals of the classical density of the initial wave packet and its time evolute during the autocorrelation examined. Apparent in this inset are the trajectories contributing to the overlap at that time step, of which a representative set is indicated by the x's, which were selected simply because they lay along the center of the overlap. Using these as the guiding trajectories for the quadratic approximation produces a rather poor fit to the exact curves. This likely remains true if one tries to capture the hairpins with two guiding trajectories each due to Gaussian wave packet overlap. On the other hand, the figure makes clear that the cubic approximation is able to reproduce this autocorrelation much more accurately with these guiding trajectories. Each contribution is added with its correct phase and amplitude relative to the others. We note that no effort was made to find the "optimal" set of guiding trajectories here. This is further evidence of the cubic approximation's relative insensitivity to appropriate guiding trajectories at some times.

VIII. CONCLUSION

We presented and examined a closed-form extension to the quadratically expanded real-trajectory time-dependent WKB formalism. We accomplished this by expanding the action $S(q,q',t)$ to third order so as to include curvature in the underlying semiclassical dynamics in phase space. The resultant expression was found to perform better than the quadratic approximation when $\hbar$ is finite, often with only one real guiding trajectory, but not so large so as to necessitate higher powers of the action.

On the negative side, for central guiding trajectories the expression was also found to behave badly at caustics, unlike the lower-order treatment, due to its prefactor not being an entire function. The cubic expression is also comparatively more sensitive to the selection of an appropriate guiding trajectory (p_t,q_t) at some times and its corresponding classical density is not always real. However, while the quadratic treatment fails at uniformly capturing the hairpins in phase space that develop with time, the cubic approximation is able to accomplish this well and is then often found to be less sensitive to the correct guiding (p_t,q_t).

Thus, overall, unlike its lower-order version, the cubic approximation proves to be very useful at effectively handling nonlinearities in phase space and is able to accomplish this without appealing to complex classical trajectory root finding or initial-value sampling of trajectories as other methods do. The derivation presented can be easily extended to higher dimensions, and we hope that it can be used as easily as the "thawed Gaussian" approximation in many-dimensional systems. Lastly, the cubic treatment we presented further solidifies the concept that underlying classical trajectories make up localized quantum wave packets, even in the nonlinear regime of dynamics, and their proper treatment can capture almost all quantum propagation.

ACKNOWLEDGMENTS

L.K. thanks the Faculty of Arts and Sciences and the Department of Chemistry and Chemical Biology at Harvard

University for generous support of this work. The authors also thank Professor Eric Heller and Steve Tomsovic for very helpful discussions, and Prof. Tomsovic and Alyssa Wilson for proofreading this paper.

APPENDIX

The coefficients in Eq. (32) are

$$\alpha = -\left[2\left(\frac{\partial^3 S}{\partial q_0^3}\right)^2\right]^{-\frac{2}{3}}\left[\left(\frac{\partial^3 S}{\partial q_0^2 \partial q_t}\right)^2 - \frac{\partial^3 S}{\partial q_0^3}\frac{\partial^3 S}{\partial q_0 \partial q_t^2}\right], \tag{A1}$$

$$\beta = 2\left[2\left(\frac{\partial^3 S}{\partial q_0^3}\right)^2\right]^{-\frac{2}{3}}\left[\frac{\partial^2 S}{\partial q_0 \partial q_t}\frac{\partial^3 S}{\partial q_0^3} - \left(\frac{\partial^2 S}{\partial q_0^2} + \frac{i\hbar}{\sigma^2}\right)\frac{\partial^3 S}{\partial q_0^2 \partial q_t}\right], \tag{A2}$$

$$\gamma = \left[2\left(\frac{\partial^3 S}{\partial q_0^3}\right)^2\right]^{-\frac{2}{3}}\left[-\left(\frac{i\hbar}{\sigma^2}\right)^2 - \left(\frac{\partial^2 S}{\partial q_0^2}\right)^2 + 2\frac{\partial^3 S}{\partial q_0^3}\left(\frac{\partial S}{\partial q_0} + \xi + \frac{i\hbar}{\sigma^2}(q_0 - q_\beta)\right) - 2\frac{i\hbar}{\sigma^2}\frac{\partial^2 S}{\partial q_0^2}\right], \tag{A3}$$

$$\delta = \frac{1}{6}\left(\frac{\partial^3 S}{\partial q_0^3}\right)^{-2}\left[2\left(\frac{\partial^3 S}{\partial q_0^2 \partial q_t}\right)^3 - 3\frac{\partial^3 S}{\partial q_0^2 \partial q_t}\frac{\partial^3 S}{\partial q_0^3}\frac{\partial^3 S}{\partial q_0 \partial q_t^2} + \left(\frac{\partial^3 S}{\partial q_0^3}\right)^2\frac{\partial^3 S}{\partial q_t^3}\right], \tag{A4}$$

$$\begin{aligned}\epsilon = \frac{1}{2}\left(\frac{\partial^3 S}{\partial q_0^3}\right)^{-2}\Bigg[&2\frac{i\hbar}{\sigma^2}\left(\frac{\partial^3 S}{\partial q_0^2 \partial q_t}\right)^2 + 2\frac{\partial^2 S}{\partial q_0^2}\left(\frac{\partial^3 S}{\partial q_0^2 \partial q_t}\right)^2 \\ &- 2\frac{\partial^2 S}{\partial q_0 \partial q_t}\frac{\partial^3 S}{\partial q_0^2 \partial q_t}\frac{\partial^3 S}{\partial q_0^3} + \frac{\partial^2 S}{\partial q_t^2}\left(\frac{\partial^3 S}{\partial q_0^3}\right)^2 - \left(\frac{i\hbar}{\sigma^2} + \frac{\partial^2 S}{\partial q_0^2}\right)\frac{\partial^3 S}{\partial q_0^3}\frac{\partial^3 S}{\partial q_0 \partial q_t^2}\Bigg],\end{aligned} \tag{A5}$$

$$\begin{aligned}\zeta = \left(\frac{\partial^3 S}{\partial q_0^3}\right)^{-2}\Bigg\{&\left(\frac{i\hbar}{\sigma^2}\right)^2\frac{\partial^3 S}{\partial q_0^2 \partial q_t} + \left(\frac{\partial^2 S}{\partial q_0^2}\right)^2\frac{\partial^3 S}{\partial q_0^2 \partial q_t} - \frac{\partial^2 S}{\partial q_0^2}\frac{\partial^2 S}{\partial q_0 \partial q_t}\frac{\partial^3 S}{\partial q_0^3} + \frac{\partial^3 S}{\partial q_0^3}\left[\frac{\partial^3 S}{\partial q_0^3}\frac{\partial S}{\partial q_t} - \frac{\partial^3 S}{\partial q_0^2 \partial q_t}\left(\frac{\partial S}{\partial q_0} + \xi\right)\right] \\ &+\frac{i\hbar}{\sigma^2}\left[2\frac{\partial^2 S}{\partial q_0^2}\frac{\partial^3 S}{\partial q_0^2 \partial q_t} - \frac{\partial^3 S}{\partial q_0^3}\left(\frac{\partial^2 S}{\partial q_0 \partial q_t} + \frac{\partial^3 S}{\partial q_0^2 \partial q_t}(q_0 - q_\beta)\right)\right]\Bigg\},\end{aligned} \tag{A6}$$

$$\begin{aligned}\eta = \frac{1}{3}\left(\frac{\partial^3 S}{\partial q_0^3}\right)^{-2}\Bigg\{&\left(\frac{i\hbar}{\sigma^2}\right)^3 + \left(\frac{\partial^2 S}{\partial q_0^2}\right)^3 + 12\left(\frac{i\hbar}{2\sigma^2}\right)^2\left(\frac{\partial^2 S}{\partial q_0^2} - \frac{\partial^3 S}{\partial q_0^3}(q_0 - q_\beta)\right) \\ &+3\frac{i\hbar}{2\sigma^2}\left[2\left(\frac{\partial^2 S}{\partial q_0^2}\right)^2 - 2\frac{\partial^2 S}{\partial q_0^2}\frac{\partial^3 S}{\partial q_0^3}(q_0 - q_\beta) + \frac{\partial^3 S}{\partial q_0^3}\left(-2\frac{\partial S}{\partial q_0} + \frac{\partial^3 S}{\partial q_0^3}(q_0 - q_\beta)^2 - 2\xi\right)\right] \\ &-3\frac{\partial^2 S}{\partial q_0^2}\frac{\partial^3 S}{\partial q_0^3}\left(\frac{\partial S}{\partial q_0} + \xi\right) + 3\left(\frac{\partial^3 S}{\partial q_0^3}\right)^2[S(q_t, q_0) + \gamma + \xi(q_0 - q_\beta)]\Bigg\}.\end{aligned} \tag{A7}$$

[1] R. P. Feynman and A. R. Hibbs, *Quantum Mechanics and Path Integrals*, Emended edition (Dover Publications, Inc., New York, 2012).

[2] L. S. Schulman, *Techniques and Applications of Path Integration* (Dover Books on Physics, Dover Publications, New York, 2012).

[3] Kenneth G. Kay, Semiclassical initial value treatments of atoms and molecules, Annu. Rev. Phys. Chem. **56**, 255 (2005).

[4] Guohua Tao and William H. Miller, Time-dependent importance sampling in semiclassical initial value representation calculations for time correlation functions, J. Chem. Phys. **135**, 024104 (2011).

[5] Guohua Tao and William H. Miller, Time-dependent importance sampling in semiclassical initial value representation calculations for time correlation functions, II. A simplified implementation, J. Chem. Phys. **137**, 124105 (2012).

[6] Shouryya Ray, Paula Ostmann, Lena Simon, Frank Grossmann, and Walter T. Strunz, Dynamics of interacting bosons using the Herman–Kluk semiclassical initial value representation, J. Phys. A: Math. Theor. **49**, 165303 (2016).

[7] Dmitrii V. Shalashilin, Nonadiabatic dynamics with the help of multiconfigurational Ehrenfest method: Improved theory and fully quantum 24d simulation of pyrazine, J. Chem. Phys. **132**, 244111 (2010).

[8] Adriano Grigolo, Thiago F. Viscondi, and Marcus A. M. de Aguiar, Multiconfigurational quantum propagation with trajectory-guided generalized coherent states, J. Chem. Phys. **144**, 094106 (2016).

[9] Bill Poirier and David Tannor, An action principle for complex quantum trajectories, Mol. Phys. **110**, 897 (2012).

[10] Jörg Tatchen, Eli Pollak, Guohua Tao, and William H. Miller, Renormalization of the frozen Gaussian approximation to the quantum propagator, J. Chem. Phys. **134**, 134104 (2011).

[11] Jiří Vaníček and Doron Cohen, Path integral approach to the quantum fidelity amplitude, Philos. Trans. R. Soc., A **374**, 20150164 (2016).

[12] Marius Wehrle, Miroslav Šulc, and Jiří Vaníček, On-the-fly ab initio semiclassical dynamics: Identifying degrees of freedom

essential for emission spectra of oligothiophenes, J. Chem. Phys. **140**, 244114 (2014).
[13] Marius Wehrle, Solène Oberli, and Jiří Vaníček, On-the-fly ab initio semiclassical dynamics of floppy molecules: Absorption and photoelectron spectra of ammonia, J. Phys. Chem. A **119**, 5685 (2015).
[14] John H. Van Vleck, The correspondence principle in the statistical interpretation of quantum mechanics, Proc. Natl. Acad. Sci. USA **14**, 178 (1928).
[15] Cécile Morette, On the definition and approximation of Feynman's path integrals, Phys. Rev. **81**, 848 (1951).
[16] Martin C. Gutzwiller, Phase-integral approximation in momentum space and the bound states of an atom, J. Math. Phys. **8**, 1979 (1967).
[17] Eric J. Heller, Time-dependent approach to semiclassical dynamics, J. Chem. Phys. **62**, 1544 (1975).
[18] E. J. Heller, Wavepacket dynamics and quantum chaology, in *Chaos et Physique Quantique/Chaos and Quantum Physics. Proc. Les Houches Summer School, Session LII 1989*, edited by M. J. Giannoni, A. Voros, and J. Zinn-Justin (North-Holland, Amsterdam, 1991).
[19] I. M. Suarez Barnes, M. Nauenberg, M. Nockleby, and S. Tomsovic, Semiclassical Theory of Quantum Propagation: The Coulomb Potential, Phys. Rev. Lett. **71**, 1961 (1993).
[20] Steven Tomsovic and Eric J. Heller, Semiclassical Dynamics of Chaotic Motion: Unexpected Long-Time Accuracy, Phys. Rev. Lett. **67**, 664 (1991).
[21] Michael F. Herman and Edward Kluk, A semiclasical justification for the use of non-spreading wavepackets in dynamics calculations, Chem. Phys. **91**, 27 (1984).
[22] E. J. Heller, Guided Gaussian wave packets, Acc. Chem. Res. **39**, 127 (2006).
[23] Daniel Huber and Eric J. Heller, Generalized Gaussian wave packet dynamics, J. Chem. Phys. **87**, 5302 (1987).
[24] Daniel Huber, Eric J. Heller, and Robert G. Littlejohn, Generalized Gaussian wave packet dynamics, Schrödinger equation, and stationary phase approximation, J. Chem. Phys. **89**, 2003 (1988).
[25] C. Chester, B. Friedman, and F. Ursell, An extension of the method of steepest descents, Math. Proc. Cambridge Philos. Soc. **53**, 599 (1957).
[26] Scipy's 0.17 Special.airy.
[27] John R. Klauder, Path integrals and stationary-phase approximations, Phys. Rev. D **19**, 2349 (1979).
[28] Eric J. Heller, Generalized theory of semiclassical amplitudes, J. Chem. Phys. **66**, 5777 (1977).
[29] Yitzhak Weissman, Semiclassical approximation in the coherent states representation, J. Chem. Phys. **76**, 4067 (1982).
[30] Michel Baranger, Marcus A. M. de Aguiar, Frank Keck, Hans-Jürgen Korsch, and Bernd Schellhaaß, Semiclassical approximations in phase space with coherent states, J. Phys. A: Math. Gen. **34**, 7227 (2001).
[31] Harinder Pal, Manan Vyas, and Steven Tomsovic, Generalized Gaussian wave packet dynamics: Integrable and chaotic systems, Phys. Rev. E **93**, 012213 (2016).
[32] Niels E. Henriksen and Eric J. Heller, Quantum dynamics for vibrational and rotational degrees of freedom using Gaussian wave packets: Application to the three-dimensional photodissociation dynamics of ICN, J. Chem. Phys. **91**, 4700 (1989).